Polydopamine Stabilized Aluminum Nanocrystals: Aqueous Stability and Benzo[a]pyrene Detection

David Renard[†,‡], *Shu Tian*[†,‡], *Arash Ahmadivand*[‡,∥], *Christopher J. DeSantis*[‡,⊥], *Benjamin D. Clark*[†,‡], *Peter Nordlander*[‡,∥,⊥], *and Naomi J. Halas**[†,‡,∥,⊥]

[†]Department of Chemistry, [‡]Laboratory for Nanophotonics, [∥]Department of Physics and Astronomy, [⊥]Department of Electrical and Computer Engineering, Rice University, 6100 Main Street, Houston, Texas 77005, United States.

Keywords aluminum, nanoparticles, polydopamine, H_2O stability, SERS detection

ABSTRACT Aluminum nanocrystals have emerged as an earth-abundant material for plasmonics applications. Al nanocrystals readily oxidize in aqueous-based solutions, however, transforming into highly stratified γ-AlOOH nanoparticles with a 700% increase in surface area in a matter of minutes. Here we show that by functionalizing Al nanocrystals with the bio-inspired polymer polydopamine, their stability in aqueous media is dramatically increased, maintaining their integrity in aqueous solution for over two weeks with no discernable structural changes. Polydopamine functionalization also provides a molecular capture layer that enables the capture of polycyclic aromatic hydrocarbon pollutants in H_2O samples and their detection by surface-enhanced Raman spectroscopy, when polydopamine-stabilized Al nanocrystal aggregates are used

as substrates. This approach was used to detect a prime carcinogenic H_2O pollutant, benzo[a]pyrene, with a sensitivity in the sub-part per billion range.

Nanoparticles with collective electron resonances, known as surface plasmons, can strongly absorb and scatter incident light at wavelengths corresponding to their plasmon resonances with optical cross-sections greater than their physical size.[1] Plasmonic nanoparticles have been utilized in a wide variety of applications. These include molecular detection, based on spectral shifts of the localized surface plasmon resonance induced by changes in local refractive index[2] or surface-enhanced Raman spectroscopy (SERS).[3–5] Other applications include plasmon-driven photocatalysis[6] and photothermal cancer therapy.[7,8] Historically, most research on plasmonic nanoparticle properties and applications has focused on Au and Ag, due to the strong optical response of Au- or Ag-constituent nanoparticles in the visible region of the spectrum, their overall chemical stability, and their ease of synthesis. For many potential applications, however, one would prefer plasmonic nanoparticles synthesized from far more earth-abundant and potentially far less expensive alternatives.[9] Al nanocrystals (Al NCs) have recently emerged as an attractive potential alternative for a variety of plasmonic nanoparticle-based applications due, at least in part, to their ability to support plasmon resonances ranging from the near infrared to the ultraviolet.[10] Colloidal, well-defined Al NCs have been synthesized with tunable resonances from 2 to 4.5 eV.[11] Al NCs have thus far been used as plasmonic photocatalysts, both as standalone photocatalysts and as the antenna in antenna-reactor photocatalyst complexes,[12,13] and as SERS substrates.[14]

A major limitation to the use of Al NCs for plasmonics applications, however, is their lack of long-term stability in aqueous solution. Unlike noble metal nanoparticles, Al NCs are

significantly more reactive, forming a 2 – 5 nm self-limiting oxide layer upon exposure to air. The oxide layer renders the nanoparticles stable in air and most organic solvents, but does not protect them from further oxidation in aqueous solution. This presents a major challenge, since many applications of plasmonic nanoparticles take place in aqueous or humid environments. One possible solution to this problem would be to functionalize the oxide surface with an additional layer. Ideally, this layer should meet the following requirements: (1) it should effectively arrest oxidation in an aqueous environment, (2) it should be sufficiently thin to avoid reducing the enhanced near field of the Al NC, an essential characteristic that enables virtually all plasmonics applications, and (3) it should be uniform enough to prevent nanoparticle aggregation and preferably support colloidal dispersal in aqueous media. The ideal modification would also provide a practical surface functionalization with chemical properties that would also facilitate plasmonics applications. Polydopamine (PDA) is a bio-inspired polymer that meets all these requirements. Its synthesis was inspired by the mussel adhesive proteins that possess a plurality of catechol and amine moieties.[15] In the past decade it has been demonstrated to be one of the most practical and useful approaches for surface functionalization due to the simplicity and versatility of its coating method, which has led to its widespread use in applications spanning many fields.[15–18] PDA is readily synthesized using a one-pot approach on a variety of substrates, with preferential deposition occurring at surfaces.[15] Because of its multiple functional groups, PDA contains regions of hydrophobic and hydrophilic character, which should allow nanoparticles to be simultaneously suspended in aqueous media and protected from oxidation and other possible undesirable chemistries.

Here we report a facile method for stabilizing Al NCs based on PDA functionalization for their dispersal and subsequent use in aqueous media. We show that PDA functionalized Al NCs are

stable in H_2O, far outlasting pristine Al NCs – by more than two weeks- with minimal structural changes, preventing the oxide growth observed in the bare Al NC case. We leverage the plasmonic Al core and the varied surface chemistry of PDA into an inexpensive SERS assay to detect a carcinogenic H_2O pollutant, benzo[a]pyrene (BaP), at the sub part-per-billion level. We also demonstrate that the Al-PDA SERS platform is capable of multicomponent PAH detection through the simultaneous detection of BaP and anthracene. Additionally, we observe and characterize a high surface area oxide structure formed when Al NCs are oxidized in high temperature H_2O which may be useful in other nanotechnological applications.

RESULTS AND DISCUSSION

Development of PDA Synthesis Compatible with Al NCs

PDA functionalization is typically accomplished by exposure to an aqueous dopamine solution buffered to basic conditions (pH 8.2-8.5) (Figure 1).[15,19] Most commonly, buffers, like Tris buffer, Bicine buffer, or phosphate buffer, are used with variable concentrations of dopamine ranging from 0.1-5 mg/mL (Figure 1A, top). This relatively mild procedure allows for the formation of PDA layers on a variety of chemically diverse substrates, including Al_2O_3.[15] However, Al NCs are susceptible to oxidation in aqueous environments, especially under acidic or basic conditions. Al_2O_3 is readily etched by both acid and base due to its amphoteric nature. When applied to Al NCs, the standard Tris-buffered method for PDA functionalization etches the Al NC core, resulting in hollow PDA shells, destroying the Al NC morphology (Figure 1B). This result would be similar in any buffered aqueous system, eliminating most published PDA syntheses for use with Al NCs. To incorporate intact Al NCs within a PDA layer, an Al-compatible synthesis scheme, employing milder nonaqueous conditions, was developed (Figure 1A, bottom). Isopropanol (IPA) was used

as the solvent during PDA functionalization in place of H_2O, and aqueous NH_4OH was used as the base catalyst in place of Tris buffer. This treatment resulted in the formation of a uniform PDA layer on the Al_2O_3 surface of the Al NCs while preserving the metallic core (Figure 1C).

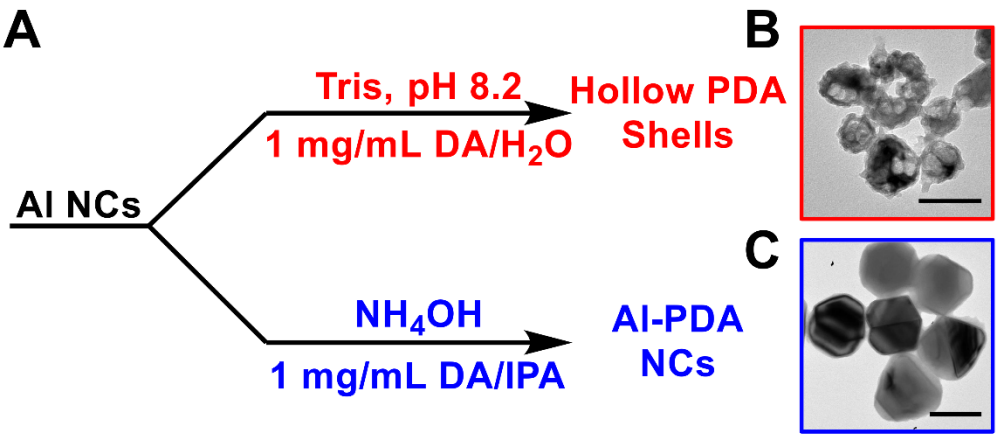

Figure 1. Development of a PDA synthesis compatible with Al NCs. (A) Standard, aqueous synthesis of PDA functionalized materials (red) and nonaqueous synthesis of PDA coated Al NCs developed in this work (blue). (B,C) Reaction products from PDA functionalization of Al NCs corresponding to the methods in (A). Scale bars are 100 nm.

Characterization of Al-PDA Composite Nanoparticles

Transmission electron microscope imaging showed that the resulting PDA layer is uniform, with a thickness of 5-7 nm, and does not obviously impact the underlying Al_2O_3 integrity or the interior Al core (Figure 2A). The thickness of the PDA layer can be tuned with reaction time in a similar manner to other PDA syntheses (Figure S1). Because the thickness of the PDA layer observed in the TEM images exceeds that of a molecular monolayer, it is most likely composed of disordered PDA chains with varying degrees of oxidation.[20] Previous studies showed that the

catechol functional group binds strongly to Al_2O_3,[21] as depicted ideally in Figure 2B for the Al NC case, however the binding mechanism is likely variable due to the disordered structure of PDA. Upon functionalization, there is a 15 nm redshift of the dipolar Al NC plasmon, because of the increased local refractive index due to the presence of the PDA coating (Figure 2C). SERS of the PDA-coated Al NCs also confirmed its surface functionalization, with prominent PDA-derived features appearing in the SERS spectrum (Figure 2D, red). 785 nm Raman excitation was used to excite a random aggregate sample of PDA coated Al NCs, in a similar manner as previously reported.[14] More details of the SERS measurement conditions are found in the experimental section. The peaks at 1490 cm^{-1} and 1276 cm^{-1} are assigned to the C=N/C=C and C-O stretches, respectively.[22] The Raman spectrum of PDA nanopowder (Figure 2D, green) shows only two broad features at 1330 cm^{-1} and 1600 cm^{-1}, which are attributed to aromatic ring stretching and deformation modes.[23] These match qualitatively to the dominating features seen in the Al-PDA SERS spectrum at 1596 cm^{-1} and 1340 cm^{-1}. We speculate the peak at 823 cm^{-1} may correspond to the Al-O-C bond formed between the Al_2O_3 and the catechol group. The peaks corresponding to PDA are always present in the SERS spectrum of the coated nanoparticle, but vary considerably in intensity and linewidth. This variability is most likely due to the random orientation of the various functional groups in the disordered PDA surface coating layer on the Al NC surface.

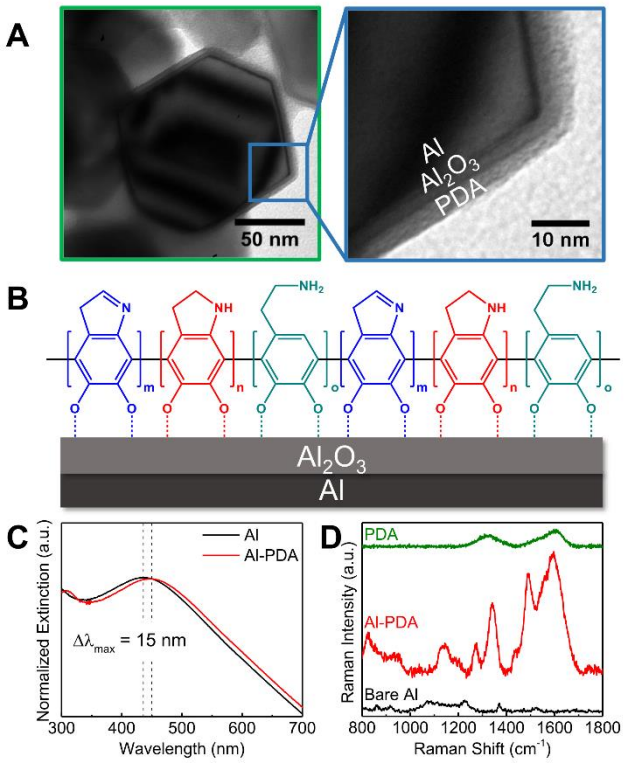

Figure 2. Characterization of PDA functionalized Al NCs. (A) TEM micrographs of PDA-modified Al NCs showing the underlying Al core, Al_2O_3 layer and carbonaceous PDA thin film. (B) Idealistic binding motif of PDA through catechol side groups. (C) Extinction spectrum of Al NCs before (black) and after (red) PDA functionalization suspended in isopropanol. (D) Comparison of the SERS spectrum of Al (black) and Al-PDA (red) with the normal Raman spectrum of powdered PDA (green).

Aqueous Stability of Bare and PDA Functionalized Al NCs

PDA functionalized Al NCs were observed to be significantly more stable under aqueous conditions than unfunctionalized Al NCs. Unfunctionalized and PDA-functionalized Al NCs were each dispersed in 20 mL of MilliQ H_2O (~3E13 particles/mL) and stirred gently at room temperature. Stirring was applied to ensure that the nanoparticles remained suspended in solution,

preventing their sedimentation, and avoiding the need for harsh sonication. TEM images and UV-Visible extinction measurements were obtained every 5 days until one of the solutions appeared to have no remaining detectable Al NCs. The unfunctionalized Al NCs began to deteriorate after about 5 days, and filamentary oxide structures began to form on their surfaces. By Day 10, the particles were very noticeably oxidized, and the metallic core began to appear oxidized as well, with the oxidized regions appearing to be pitted. By Day 15, no metallic Al was visible in the TEM images of the unfunctionalized NC sample (Figure 3A, bottom). In contrast, for the same period of aqueous exposure, the PDA-functionalized Al NCs appeared to remain as well-defined nanoparticles, with no noticeable oxide formation or pitting of the Al NC core (Figure 3A, top). The protecting effect of PDA was observed throughout the sample, with no generation of oxide strands observable in TEM imaging over large areas and many particles (Figure S2). We note that the aggregation state of the PDA-functionalized Al NCs and the particle surface roughness increased throughout the 15 days in water (Figure S2). We believe the increase in aggregation may be due to structural changes as the PDA layer is hydrated and the lack of sonication throughout the experiment. Sonication was avoided to prevent premature oxidation or disruption of the PDA coating. The oxidation process was also monitored by the disappearance of the Al plasmon peak, with a 98.7% loss in optical density by Day 15 (Figure 3B). The difference between the functionalized and unfunctionalized Al NC oxidation is clearly visible by eye by Day 15 (Figure 3B inset). Although the observed optical density of the PDA-functionalized Al NC solution decreased slightly (16.4%) through the course of the experiment, there were no oxide products observable in the TEM images (Figures 3 and S2). We therefore attribute this observed decrease to the small amount of PDA-functionalized Al NCs adsorbed onto the Teflon stir bar throughout the duration of the study and to the increase in aggregation observed in TEM imaging (Figure S2).

The slight redshift of the Al plasmon (Figure S3) also implies an increase in aggregation throughout the 15 days in H_2O. Regardless of these factors, PDA functionalization unambiguously improves aqueous stability of Al NCs.

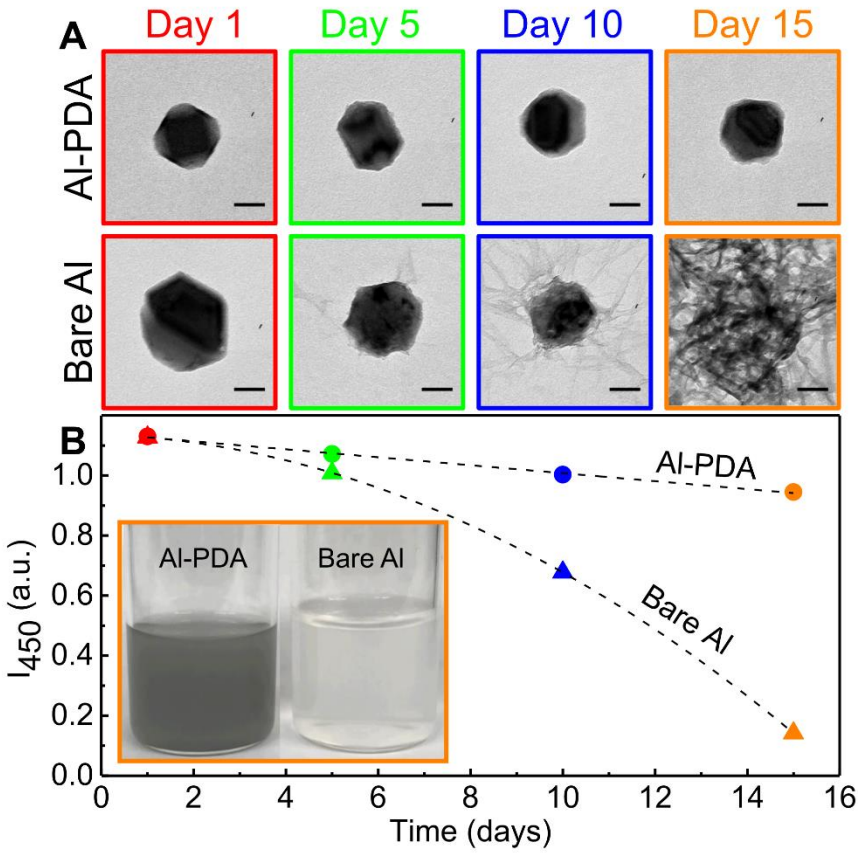

Figure 3. Room temperature oxidation study of Al and Al-PDA dispersed in aqueous solution. (A) TEM micrographs of individual particles of Al-PDA NCs (top) and bare Al NCs (bottom) at regular intervals during H_2O exposure. Scale bars are 50 nm. (B) Extinction intensity at 450 nm for bare and PDA functionalized Al NCs monitored at intervals corresponding to images in (A). Inset shows photographs of Al-PDA (left) and Al (right) aqueous suspensions after 15 days.

Al-PDA for Polycyclic Aromatic Hydrocarbon Detection

The greatly enhanced aqueous stability of PDA-functionalized Al NCs allows for their use in a variety of applications compatible with aqueous environments. Having previously demonstrated the utility of unfunctionalized Al NC aggregates as sustainable SERS substrates,[14] we now examine PDA-functionalized Al NCs for SERS-based analytical applications,[24–26] where the PDA coating acts as a molecular capture layer. Polycyclic aromatic hydrocarbons (PAHs) are a class of H_2O pollutants, 16 of which are recognized by the United States Environmental Protection Agency as priority chemical contaminants, and are often found at low concentrations in polluted H_2O.[27] These planar compounds are composed of fused benzene rings that are generated by the incomplete combustion of carbonaceous material, produced during oil refinery and waste incineration.[28] They can be found in air, H_2O and soils/sediment and linger in the environment at low levels due to their hydrophobic and unreactive structure. Most PAHs are recognized as carcinogens due to their ability to bind DNA during metabolic breakdown and promote tumor growth.[28] Benzo[a]pyrene (BaP) is one of the most carcinogenic members of the PAH family and is listed as a group 1 carcinogen by the International Agency for Research on Cancer (IARC). BaP levels at any concentration can pose a significant environmental and human health threat. Currently, PAH detection involves the use of lab-based analytical techniques, such as high-pressure liquid chromatography (HPLC)[29] and mass spectrometry (MS)[30] but requires significant sample preparation, large sample volumes, and expensive detectors. Additionally, none of the established PAH detection methods are fieldable, requiring samples to be lab-analyzed which is costly and sluggish. SERS substrates using Au and Ag have also been investigated for the detection of PAH molecules and can reach limits of detection in the hundreds of pM range, typically requiring very specific surface modifications such as self-assembled monolayers (SAMs).[31]

The multifunctional nature of PDA and the plasmonic properties of Al NCs are a particularly well-suited combination for the detection of PAH contaminants in H_2O. The hydrophobic domains formed by the aromatic units comprising the PDA layer can trap PAH molecules at Al NC surfaces, placing them within the "hot-spots" of an Al NC aggregate SERS substrate.[32] Unlike lithographically fabricated SERS substrates, the Al-PDA system consists of random aggregates (Figure 4A), yielding a wide range of particle-particle geometries and hot spot profiles. We utilized Al NCs with an average size of 125 nm based on FDTD simulations modelling the scattering profile and electric field maps of PDA functionalized octahedral Al dimers (Figure 4B-C). Particles with diameters between 115 and 130 nm are predicted to give strong field enhancements under 785 nm illumination used during SERS measurements. Since SERS enhancement scales with $|E|^4$, matching the optical response of the particles to the Raman pump is crucial for optimal sensing performance. The dark-field scattering spectrum of the Al-PDA aggregates on a quartz substrate shows a slightly red-shifted spectral peak compared to the simulated dimer scattering of 130 nm particles (Figure S4). We attribute this to the non-uniformity in particle size within the sample, the morphological differences between a perfect edge-to-edge dimer and a random aggregate, and the larger contributions to the scattering spectrum from the largest particles. From the experimental scattering spectrum, 785 nm excitation is predicted to give the better SERS enhancements over other common Raman pumps like 532 or 633 nm. The combination of dispersive liquid-liquid microextraction and the SERS sensitivity of this substrate allow for very low limits of detection. To prepare samples, a dilute contaminated H_2O sample was concentrated with a microvolume of C_2Cl_4, then dried onto an Al-PDA random aggregate SERS substrate for detection on a quartz slide (Figure 4D). Each SERS substrate (Figure 4E) uses only 10 μL of

concentrated Al-PDA solution, enabling the fabrication of thousands of substrates from one typical Al synthesis reaction.

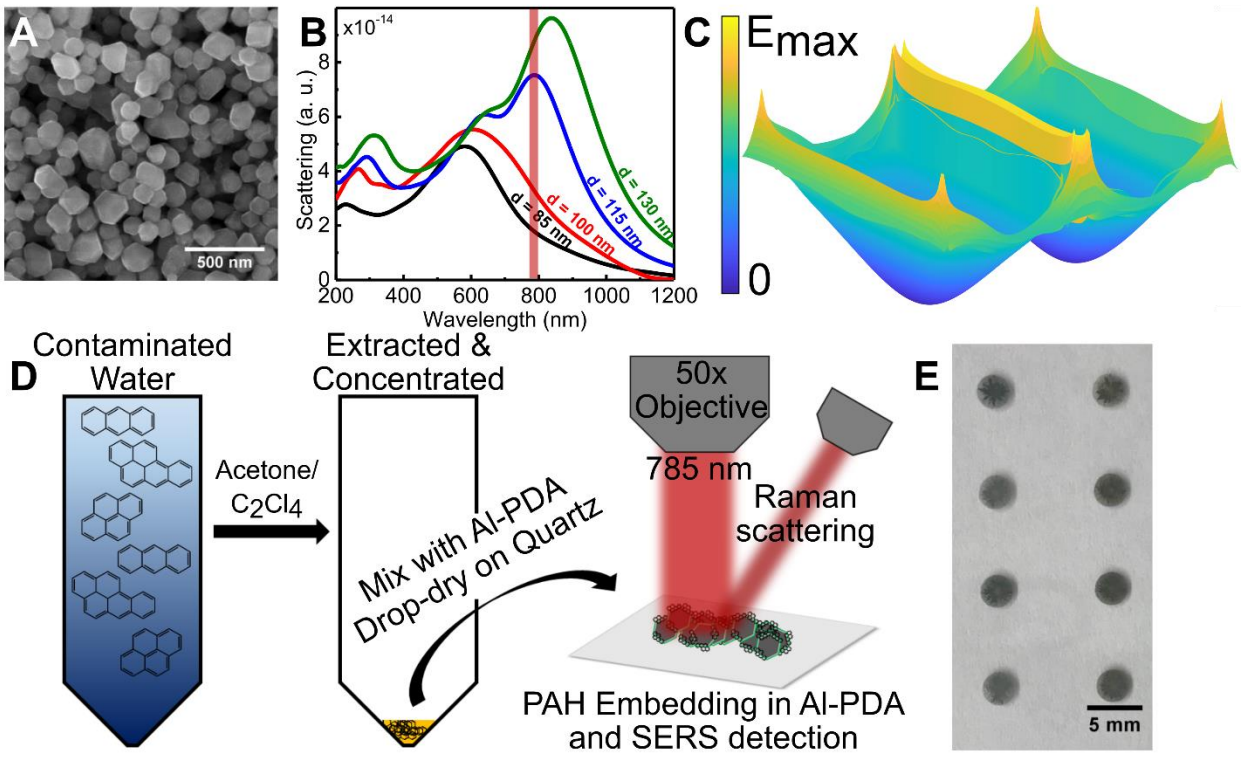

Figure 4. Al-PDA substrates paired with C_2Cl_4 dispersive liquid-liquid microextraction as a SERS platform for PAH detection. (A) SEM image of aggregated Al-PDA particles used as SERS substrates. (B) Simulated single particle scattering of an Al dimer composed of two octahedral nanocrystals facing edge to edge with a 4 nm oxide shell and an interparticle gap of 12 nm filled with PDA. The red bar at 785 nm represents the Raman pump used in SERS measurements. (C) The 3-dimensional electric field map of a dimer (d = 115 nm) when excited at 785 nm corresponding to the blue spectrum in (B). (D) Schematic depicting microextraction and Al-PDA based SERS detection of PAH contaminated H_2O. (E) Image of Al aggregates on quartz substrate used for PAH detection.

The SERS features of the PDA layer are minimally affected by the C_2Cl_4 extraction solvent, indicating little structural change in the polymer coating. Additionally, the extraction process does not interfere with the identification of the characteristic BaP peaks in the SERS spectrum (Figure 5A). The normal Raman spectrum of BaP has two predominant peaks at 1240 cm^{-1} and 1385 cm^{-1} (Figure 5A) corresponding to C-H in-plane bending and aromatic C-C stretching modes, respectively.[33] The peak at 1385 cm^{-1} appears at the shoulder of a large PDA peak at 1345 cm^{-1}, so the BaP peak at 1240 cm^{-1} was chosen for detection, despite its lower intensity. We also performed a control experiment consisting of BaP SERS detection using bare Al NC aggregates (Figure S5). We observe no discernable peak at 1240 cm^{-1} and only a minor feature at 1385 cm^{-1} using unfunctionalized Al NCs, highlighting the effectiveness of PDA-enabled BaP enrichment in the "hot spots" of the SERS substrate. By plotting the SERS intensity of the BaP peak at 1240 cm^{-1} against the concentration of BaP in the original H_2O sample, BaP can be reliably detected down to 7.93 nM (2.00 ppb) (Figure 5B). The data follows a Langmuir model, indicative of hot-spot saturation by BaP at high concentrations. To estimate the limit of detection of this system, the Langmuir fit was extrapolated to a signal-to-noise ratio (SNR) of three, yielding a limit of detection of 2.11 nM (0.532 ppb) (Figure 5C). If we instead extrapolate to a SNR of two, the limit of detection is lowered to 0.310 ppb. The baseline was determined using the signal obtained at 1240 cm^{-1} of an identically prepared Al-PDA SERS substrate with no BaP analyte exposure. The noise level was estimated using the standard deviation of the signal in the 1700 – 1800 cm^{-1} region where no Raman features are observed. The standard deviation in this region was computed for the 21 measurements comprising the data in Figure 5C and used as an estimation of the noise throughout the acquisition region. This noise estimation was used to calculate the SNR thresholds shown in Figure 5C. We also evaluate the Al-PDA SERS platform for multicomponent detection by

simultaneously detecting anthracene (Anth) and BaP (Figure 5D). The identifying peaks of both BaP, at 1240 cm^{-1}, and Anth, at 1407 cm^{-1}, can be easily distinguished from the PDA background at a total PAH concentration of 0.2 ppm. This demonstration indicates the feasibility of implementing Al-PDA SERS substrates with realistic PAH polluted samples where the detection of many PAH species would be necessary. This sensitive PAH-sensing platform could be applied to other contaminated systems, such as detecting polychlorinated biphenyls or the sensing multiple PAH species simultaneously. The low sampling volumes required and ease of substrate fabrication make this SERS assay a straightforward fieldable analytical tool.

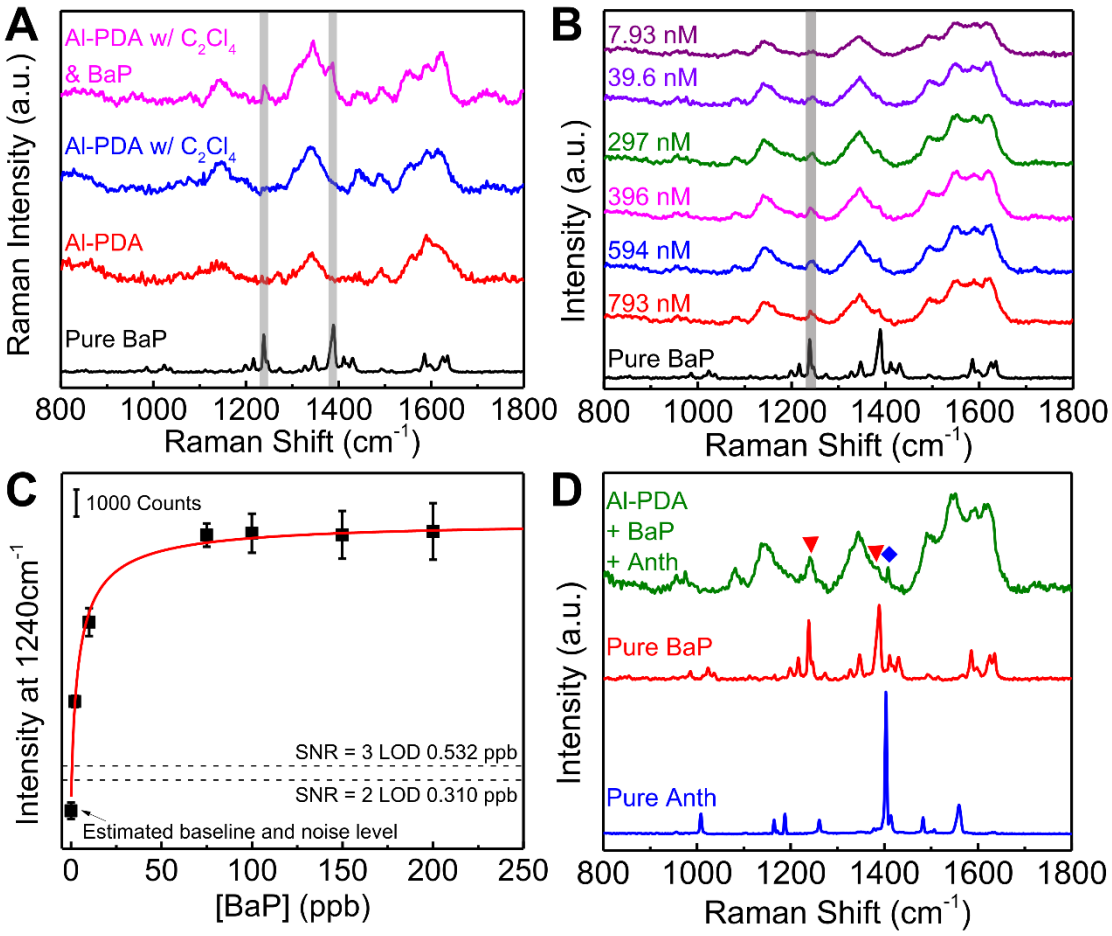

Figure 5. (A) Raman spectrum of pure BaP (black) and SERS spectra of the Al-PDA aggregate substrate (red), Al-PDA substrate treated with 10 µL of C_2Cl_4 extraction solvent (blue), and Al-

PDA substrates treated with 10 μL of BaP enriched C_2Cl_4 extract (pink). BaP peaks of interest are marked with gray bars. (B) SERS spectra of Al-PDA aggregate substrates with BaP extracted from H_2O (793 – 7.93 nM) using C_2Cl_4 and normal Raman spectrum of BaP. (C) SERS signal as a function of BaP concentration in original H_2O sample determined using the peak at 1240 cm^{-1} fit with a Langmuir model. Each point is the average of three measurements and error bars are reported as the standard error of the mean. (D) Simultaneous detection of Anth and BaP (green) using Al-PDA SERS substrates. Normal Raman spectra of BaP (red) and Anth (blue) are shown as reference. Matching peaks are indicated with red triangles (BaP) and blue diamonds (Anth).

High Temperature Stability of Al-PDA

To explore the effectiveness of PDA-enabled oxidation protection, we investigated the stability of PDA functionalized Al NCs in high temperature H_2O. The stability of PDA functionalized Al NCs was evaluated in a similar method to the room temperature case discussed previously using a stirred, heated cuvette stage. The dipole plasmon peak was monitored throughout the oxidation process and TEM samples were made after the oxidation had finished. Both bare and PDA functionalized Al NCs exhibited a similar sigmoidal oxidation behavior (Figure 6A) with an induction period followed by a rapid decrease in optical intensity corresponding to Al oxidation. The similar sigmoidal oxidation behavior implies the same underlying oxidation mechanism and that PDA surface functionalization simply delays oxidation onset. Here we refer to the inflection point in the sigmoidal oxidation plot as the oxidation time, to fairly compare the oxidation behavior at different temperatures (Figure S6). At these high temperatures, PDA-functionalized Al NCs consistently outperformed the bare NCs, however both samples oxidized at a rate that increased with increasing temperature (Figure 6B). Additionally, the benefit of PDA functionalization on preventing Al NC oxidation decreased with increasing temperature, suggesting that PDA

functionalization is a more effective treatment for lower temperature conditions. Bare Al NCs and PDA functionalized particles yield similar oxidation products (Figure 6C-D), further supporting the hypothesis that PDA modification postpones Al oxidation but does not alter the underlying mechanism.

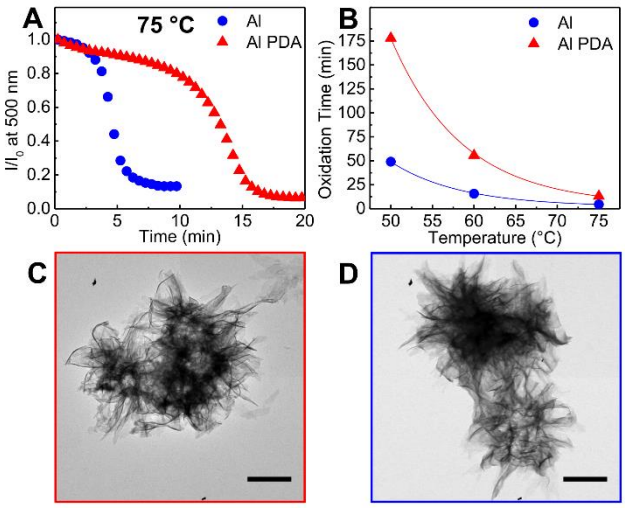

Figure 6. High temperature oxidation study of Al and Al-PDA dispersed in H_2O. (A) I/I_0 of a 75 ^{0} C aqueous dispersion of Al (blue) and Al-PDA (red) monitored by UV-vis at 500 nm. (B) Oxidation time for Al (blue) and Al-PDA (red) at three H_2O temperatures (50, 60, and 75 ^{0} C). TEM micrographs of Al (C) and Al-PDA (D) after dispersion in 75 ^{0} C corresponding to the endpoints in (A). Scale bars are 200 nm.

Characterization of Oxidized Al NCs

The morphology of the fully oxidized Al_2O_3 nanoparticles is strongly influenced by the temperature of the aqueous solution during the oxidation reaction (Figure 7). Al NCs oxidized in pH neutral MilliQ H_2O at elevated temperatures formed high-surface-area oxide nanoparticles. Powder X-Ray Diffraction (XRD) confirmed that all metallic Al had been consumed and that the

structures are composed of γ-AlOOH, but are of limited crystallinity (Figure 7A and S7). Energy dispersive X-Ray spectroscopy (EDS) confirmed a composition of only Al and O (Figure S8). These structures are more particulate than the room temperature case, with those synthesized at 75 °C being the most discrete (Figure 7 B-E). In both the 60 and 75 °C cases, the hollow center of each oxide particle corresponds to the predecessor Al NC (or cluster of NCs). UV-Vis of the sample before and after oxidation in 75 °C H_2O shows a complete loss of the Al dipole at 440 nm, confirming that all metallic Al has been consumed (Figure 7F). Nitrogen adsorption-desorption measurements (Figure 7G) of the oxide product displays unhindered gas adsorption at high P/P_0 and a hysteresis loop, suggesting aggregates of nano-sheet or platelet morphology with slit-like pores,[34] consistent with TEM and SEM analysis (Figure 7E and S3). Brunauer–Emmett–Teller measurements (Figure S9) revealed that the surface area of the oxide product is almost 7x larger than Al NCs, with surface areas of 356.903 m^2/g and 53.128 m^2/g respectively, comparable to AlOOH nanostructures prepared from other precursor nanoparticles[35–37] and within a factor of 3 of Al-based metal-organic frameworks such as MIL-53(Al).[38]

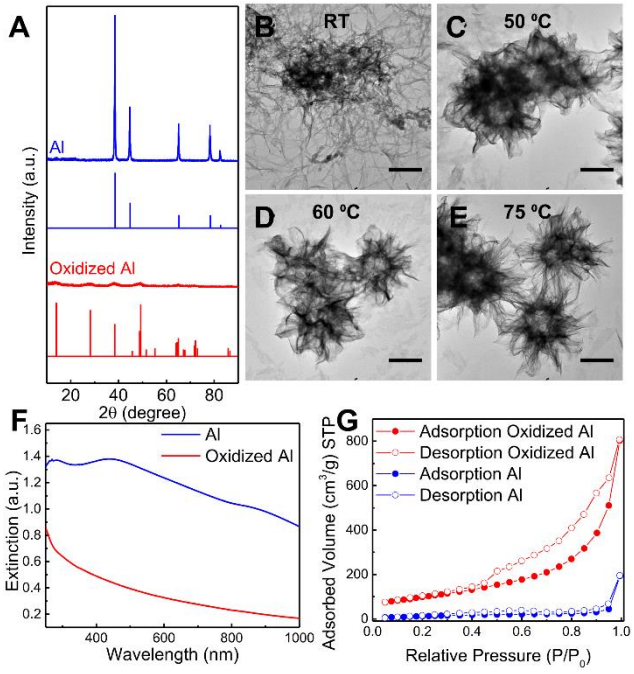

Figure 7. Characterization of oxidized Al NCs. (A) Powder XRD of Al NCs (blue) and oxidized Al NCs (red) and matching XRD library entries for Al and γ-AlOOH (Boehmite), respectively. (B-E) TEM micrographs of Al NCs oxidized at room temperature, 50, 60, 75 ^{0} C. Scale bars are 200 nm. (F) Extinction spectrum of Al NCs (blue) and Al oxidized in 75 ^{0} C H_2O for 20 minutes (red). (G) Nitrogen adsorption-desorption of Al NCs (blue) and Al NCs oxidized in 75 ^{0} C H_2O (red).

CONCLUSION

In summary, a method for functionalizing Al NCs with an ultra-thin PDA layer was developed using isopropanol and NH_4OH. This procedure dramatically improves the stability of Al NCs in H_2O, preventing their oxidation, and preserving their optical properties after two weeks in aqueous solution. Without PDA functionalization, high surface area γ-AlOOH particles are

formed by mild-temperature oxidation of Al NCs in H_2O, with a ~7x increase in surface area which may be useful for filtration or catalyst support applications. By leveraging the hydrophobic properties of a PDA layer with the plasmonic Al NC core, we have developed a rapid, inexpensive SERS-based detection platform for PAH contaminants in H_2O samples with a sensitivity of 2.11 nM (0.532 ppb). We have also shown the feasibility of multicomponent pollutant analysis, detecting both BaP and Anth simultaneously. While this work demonstrates one specific use for PDA functionalized Al NCs, we believe that the combination of H_2O-stable Al NCs and the multifunctional nature of PDA will lead to multiple applications of colloidal Al NCs as an earth-abundant, inexpensive plasmonic system for fieldable nanosensing applications.

EXPERIMENTAL SECTION

Materials. Anhydrous tetrahydrofuran, anhydrous dioxane, N,N-dimethylethylamine alane (0.5M in toluene), titanium (IV) isopropoxide (99.999%), anhydrous toluene, dibutylphosphate (97%), anhydrous cyclohexane, isopropanol (ACS grade), dopamine hydrochloride, NH_4OH (28-30% in H_2O), benzo[a]pyrene (≥96%), tetrachloroethylene (≥99.9%), methanol (ACS grade), acetone (HPLC grade), and anthracene (99%) were obtained from Millipore Sigma and used without further purification. Silicone spacers (2.5 mm diameter, 2 mm depth) were obtained from Thermo fisher.

Characterization. TEM imaging was performed using a 1230 JEOL High Contrast TEM operating at 80 kV. High resolution TEM imaging was performed using a 2100F JEOL TEM operating at 200 kV. SEM imaging and EDS analysis was performed using a FEI Helios Nanolab 660 DualBeam. Dark-field scattering measurements were performed on a Zeiss microscope coupled with a Princeton Instrument SP2150 spectrometer and a CCD detector. N_2 adsorption-

desorption and BET measurements were performed on dry powders of Al NCs or oxidized Al NCs using a Quantachrome Autosorb-iQ-MP/Kr BET Surface Analyzer. XRD analysis was performed on powdered Al NCs and oxidized Al NCs using a Rigaku D/Max Ultima II. All Raman/SERS spectra were measured using a Renishaw in*Via* Raman microscope using a 50x air objective. SERS samples were prepared by adding 10 μL of either Al or Al-PDA NCs dispersed in IPA onto quartz substrates and allowing them to dry under vacuum. Spectra were measured in ambient atmosphere using 785 nm excitation with a 2 by 2 μm spot size and 0.038 mW laser power. SERS spectra are averaged over 25 scans using 40 s integration time.

Synthesis of Al NCs. Al NCs were synthesized using previously established protocol with slight modification.[11] Briefly, a 2:3 v/v mixture of anhydrous THF/dioxane (Sigma) totaling 25 mL was heated to 40 ^{0} C in an air-free flask under argon. Once heated, 6 mL of 0.5 M dimethylethylamine alane in toluene (Sigma) was added *via* syringe and the mixture was allowed to stir rapidly for 3 minutes. Then, 0.5 mL of 1% (v/v) titanium (IV) isopropoxide (Sigma) in anhydrous toluene was added rapidly *via* syringe. The reaction was stirred for 2 hours at 40 ^{0} C and under argon, during which the reaction became opaque and gray. Then, 5 mL of 1% (v/v) dibutylphosphate in cyclohexane was added. The reaction was opened to atmosphere and dispersed into toluene, separated by centrifugation and redispersed in isopropanol *via* sonification for three cycles. Final volume was kept at 25 mL.

PDA Functionalization. Polydopamine functionalization was accomplished 5 mL of washed Al NCs were centrifuged to remove the isopropanol. The sample was redispersed in 50 mL of 1 mg/mL dopamine HCl in isopropanol. The reaction was vigorously stirred and 1.25 mL aqueous NH_4OH was added. The reaction was allowed to stir for 6 hours. The particles were centrifuged and redispersed twice in fresh IPA to remove residual reagents.

Simulations of Al-PDA SERS Substrates. To understand and predict the spectral response and properties of Al octahedral nanoparticles, we carried out 3D finite-difference time-domain (FDTD) analysis (using Lumerical 2018 package). Using empirically measured dielectric constants for Al by Palik,[39] it is assumed that the nanoparticles are covered with Al_2O_3 coverage with the thickness of 4 nm and all are deposited on a quartz substrate with the relative permittivity of ε=2.1. The refractive index of PDA coating is assumed to be 1.6.[40] The spatial grid cell sizes in all axes are set to $\Delta x=\Delta y=\Delta z$=0.6 nm for meshing the structures, and the time step is set as $dt\sim$ 0.01 fs, to ensure about the Courant stability for all wavelengths and employed materials in the workplace.[41] The simulation area is bounded by 48 sheets of perfectly matched layers (PML) to absorb propagating and evanescent beams with marginal reflections to the workplace.

BaP SERS Detection. BaP detection with Al-PDA SERS substrates was accomplished by drop casting 10 µL of PDA functionalized Al NCs on a quartz slide using a silicone spacer (2.5 x 2.5 x 2 mm well size). The silicone spacer was removed after the sample had dried and 5 µL of BaP-enriched C_2Cl_4 was dropped on each Al-PDA aggregate and allowed to dry. The BaP-enriched C_2Cl_4 was made by diluting 50 µL of BaP/methanol stock solutions (ranging from 200 – 2 mg/L) into 49.95 mL of MilliQ H_2O. To this, 1 mL of dispersing solvent (600 µL C_2Cl_4 and 30 mL acetone) was added and vortexed. Then, this sample was centrifuged at 3000xg for 3 minutes, leaving a small droplet of BaP-enriched C_2Cl_4 which was then collected with a micropipette. SERS measurements were collected in ambient atmosphere using 785 nm excitation with a 2 by 2 µm spot size and 0.19 mW laser power. Spectra were averaged over 25 scans using 40 s integration time and measured using a Renishaw in*Via* Raman microscope using a 50x air objective.

Simultaneous BaP and Anth SERS Detection. BaP and Anth were simultaneously detected using Al-PDA SERS substrates in a similar manner to BaP alone. 50 µL of both BaP and Anth methanol

stock solutions (50 mg/L) were spiked into 49.9 mL of MilliQ H_2O. To this, 1 mL of dispersing solvent was added and vortexed. The extracted PAH mixture was collected by centrifugation and 5 μL was drop-dried on top of Al-PDA aggregates on a quartz slide. SERS measurements were performed in the same manner as BaP alone.

High Temperature H_2O Stability. 2.5 mL of MilliQ H_2O was added to a quartz cuvette on a temperature-controlled cuvette stage equipped with a magnetic stirrer. Once the temperature stabilized, a blank was taken at the dipolar plasmon peak of the Al NCs (~450 nm). 500 μL of Al NCs or Al-PDA NCs dispersed in H_2O were rapidly added and the intensity at the dipolar mode was measured continuously until the solution was clear and the intensity at the monitored wavelength stopped changing. The oxidation of the particles follows a sigmoidal curve, with a slow decay followed by a sharp drop in absorbance intensity and then no further decrease. Al NCs or Al PDA NCs were monitored at three different temperatures, 50, 60, and 75 ^{0} C. The obtained kinetic curves were fit to a sigmoidal curve. This simulated curve was then differentiated to obtain the inflection point (minima in the differential plot). This inflection point was deemed the point at which the sample was oxidized and no longer viable.

Synthesis of Oxidized Al Nanoparticles. Oxidized Al NCs were synthesized by rapidly injecting 0.5 mL of Al NCs dispersed in H_2O into a rapidly stirring vial of MilliQ H_2O at the desired temperature and allowing to stir until all traces of gray were gone (variable based on temperature). The white precipitate was collected *via* centrifugation and washed twice in fresh IPA. This procedure was scaled up 10x for XRD and BET sample preparation.

ASSOCIATED CONTENT

Supporting Information.

Detailed explanations for the scattering profiles and E-field maps used in theoretical modeling. Example of sigmoidal fitting procedure used for high temperature oxidation analysis. TEM image and corresponding selected-area electron diffraction from oxidized Al NCs. SEM-EDS analysis of oxidized Al NCs and high resolution TEM imaging of oxidized Al NCs. Multi-point BET plots of Al NCs and oxidized Al NCs used for surface area calculations. This material is available free of charge *via* the Internet at http://pubs.acs.org. (PDF) The authors declare no competing financial interest.

AUTHOR INFORMATION

Corresponding Author

*E-mail: halas@rice.edu

Author Contributions

N.J.H. supervised the research and advised in project direction. D.R. performed all experiments and wrote the manuscript. A.A. performed theoretical modeling and simulation. P.N. advised and gave input to theoretical computation. S.T. helped with Raman measurements, dark-field scattering measurements, and data processing. S.T., C.J.D., and B.D.C. assisted with project direction, manuscript preparation, and editing. All authors read the manuscript and contributed to the final version and presentation of the work.

ACKNOWLEDGMENTS

This work was supported by ARO (W911NF-12-1-0407), AFOSR (FA9550-15-1-0022), the Welch Foundation (C-1220, NJH), NSF (EEC-1449500) and DTRA (HDTRA1-16-1-0042). D.R. was supported by the Department of Defense (DoD) through the National Defense Science & Engineering Graduate Fellowship (NDSEG) Program.

REFERENCES

(1) Bohren, C. F. How Can a Particle Absorb More than the Light Incident on It? *Am. J. Phys.* **1983**, *51*, 323–327.

(2) Mayer, K. M.; Hafner, J. H. Localized Surface Plasmon Resonance Sensors. *Chem. Rev.* **2011**, *111*, 3828–3857.

(3) Stiles, P. L.; Dieringer, J. A.; Shah, N. C.; Van Duyne, R. P. Surface-Enhanced Raman Spectroscopy. *Annu. Rev. Anal. Chem.* **2008**, *1*, 601–626.

(4) Li, J. F.; Huang, Y. F.; Ding, Y.; Yang, Z. L.; Li, S. B.; Zhou, X. S.; Fan, F. R.; Zhang, W.; Zhou, Z. Y.; Wu, D. Y.; Ren, B.; Wang, Z. L.; Tian, Z. Q. Shell-Isolated Nanoparticle-Enhanced Raman Spectroscopy. *Nature* **2010**, *464*, 392–395.

(5) Wei, H.; Xu, H. Hot Spots in Different Metal Nanostructures for Plasmon-Enhanced Raman Spectroscopy. *Nanoscale* **2013**, *5*, 10794–10805.

(6) Christopher, P.; Xin, H.; Linic, S. Visible-Light-Enhanced Catalytic Oxidation Reactions on Plasmonic Silver Nanostructures. *Nat. Chem.* **2011**, *3*, 467–472.

(7) Hirsch, L. R.; Stafford, R. J.; Bankson, J. A.; Sershen, S. R.; Rivera, B.; Price, R. E.; Hazle, J. D.; Halas, N. J.; West, J. L. Nanoshell-Mediated near-Infrared Thermal Therapy of

Tumors under Magnetic Resonance Guidance. *Proc. Natl. Acad. Sci.* **2003**, *100*, 13549–13554.

(8) Anastos, H.; Winoker, J.; Shukla, P.; Cumarasamy, S.; Sfakianos, J.; Carrick, M.; Rastinehad, B.; Knauer, C.; Taouli, B.; Lewis, S.; Schwartz, J.; Rastinehad, A. PD65-04 MR/US FUSION GUIDED ULTRA-FOCAL GOLD NANOPARTICLE DIRECTED LASER ABLATION OF PROSTATE TUMORS: RESULTS IN THE FIRST 11 PATIENTS (PHASE I/II TRIAL). *J. Urol.* **2018**, *199*, e1226.

(9) Zorić, I.; Zäch, M.; Kasemo, B.; Langhammer, C. Gold, Platinum, and Aluminum Nanodisk Plasmons: Material Independence, Subradiance, and Damping Mechanisms. *ACS Nano* **2011**, *5*, 2535–2546.

(10) Knight, M. W.; King, N. S.; Liu, L.; Everitt, H. O.; Nordlander, P.; Halas, N. J. Aluminum for Plasmonics. *ACS Nano* **2014**, *8*, 834–840.

(11) McClain, M. J.; Schlather, A. E.; Ringe, E.; King, N. S.; Liu, L.; Manjavacas, A.; Knight, M. W.; Kumar, I.; Whitmire, K. H.; Everitt, H. O.; Nordlander, P.; Halas, N. J. Aluminum Nanocrystals. *Nano Lett.* **2015**, *15*, 2751–2755.

(12) Zhou, L.; Zhang, C.; McClain, M. J.; Manjavacas, A.; Krauter, C. M.; Tian, S.; Berg, F.; Everitt, H. O.; Carter, E. A.; Nordlander, P.; Halas, N. J. Aluminum Nanocrystals as a Plasmonic Photocatalyst for Hydrogen Dissociation. *Nano Lett.* **2016**, *16*, 1478–1484.

(13) Swearer, D. F.; Zhao, H.; Zhou, L.; Zhang, C.; Robatjazi, H.; Martirez, J. M. P.; Krauter, C. M.; Yazdi, S.; McClain, M. J.; Ringe, E.; Carter, E. A.; Nordlander, P.; Halas, N. J. Heterometallic Antenna−reactor Complexes for Photocatalysis. *Proc. Natl. Acad. Sci.* **2016**,

113, 8916–8920.

(14) Tian, S.; Neumann, O.; McClain, M. J.; Yang, X.; Zhou, L.; Zhang, C.; Nordlander, P.; Halas, N. J. Aluminum Nanocrystals: A Sustainable Substrate for Quantitative SERS-Based DNA Detection. *Nano Lett.* **2017**, *17*, 5071–5077.

(15) Lee, H.; Dellatore, S. M.; Miller, W. M.; Messersmith, P. B. Mussel-Inspired Surface Chemistry for Multifunctional Coatings. *Science* **2007**, *318*, 426–430.

(16) Zhou, J.; Xiong, Q.; Ma, J.; Ren, J.; Messersmith, P. B.; Chen, P.; Duan, H. Polydopamine-Enabled Approach toward Tailored Plasmonic Nanogapped Nanoparticles: From Nanogap Engineering to Multifunctionality. *ACS Nano* **2016**, *10*, 11066–11075.

(17) Ryu, J.; Ku, S. H.; Lee, H.; Park, C. B. Mussel-Inspired Polydopamine Coating as a Universal Route to Hydroxyapatite Crystallization. *Adv. Funct. Mater.* **2010**, *20*, 2132–2139.

(18) Ryu, J. H.; Messersmith, P. B.; Lee, H. Polydopamine Surface Chemistry: A Decade of Discovery. *ACS Appl. Mater. Interfaces* **2018**, *10*, 7523–7540.

(19) Sheng, W.; Li, B.; Wang, X.; Dai, B.; Yu, B.; Jia, X.; Zhou, F. Brushing up from "Anywhere" under Sunlight: A Universal Surface-Initiated Polymerization from Polydopamine-Coated Surfaces. *Chem. Sci.* **2015**, *6*, 2068–2073.

(20) Liebscher, J.; Mrówczyński, R.; Scheidt, H. A.; Filip, C.; Haìdade, N. D.; Turcu, R.; Bende, A.; Beck, S. Structure of Polydopamine: A Never-Ending Story? *Langmuir* **2013**, *29*, 10539–10548.

(21) Borah, J. M.; Sarma, J.; Mahiuddin, S. Adsorption Comparison at the α-Alumina/Water Interface: 3,4-Dihydroxybenzoic Acid vs. Catechol. *Colloids Surfaces A Physicochem. Eng. Asp.* **2011**, *387*, 50–56.

(22) Luo, H.; Gu, C.; Zheng, W.; Dai, F.; Wang, X.; Zheng, Z. Facile Synthesis of Novel Size-Controlled Antibacterial Hybrid Spheres Using Silver Nanoparticles Loaded with Poly-Dopamine Spheres. *RSC Adv.* **2015**, *5*, 13470–13477.

(23) Fei, B.; Qian, B.; Yang, Z.; Wang, R.; Liu, W. C.; Mak, C. L.; Xin, J. H. Coating Carbon Nanotubes by Spontaneous Oxidative Polymerization of Dopamine. *Carbon N. Y.* **2008**, *46*, 1795–1797.

(24) Silva, W. R.; Graefe, C. T.; Frontiera, R. R. Toward Label-Free Super-Resolution Microscopy. *ACS Photonics* **2016**, *3*, 79–86.

(25) Kumar, S.; Kumar, A.; Kim, G. H.; Rhim, W. K.; Hartman, K. L.; Nam, J. M. Myoglobin and Polydopamine-Engineered Raman Nanoprobes for Detecting, Imaging, and Monitoring Reactive Oxygen Species in Biological Samples and Living Cells. *Small* **2017**, *13*, 1–10.

(26) Vangala, K.; Yanney, M.; Hsiao, C.-T.; Wu, W. W.; Shen, R.-F.; Zou, S.; Sygula, A.; Zhang, D. Sensitive Carbohydrate Detection Using Surface Enhanced Raman Tagging. *Anal. Chem.* **2010**, *82*, 10164–10171.

(27) US EPA. Priority Pollutant List. **2014**, Priority Pollutant List.

(28) Abdel-Shafy, H. I.; Mansour, M. S. M. A Review on Polycyclic Aromatic Hydrocarbons: Source, Environmental Impact, Effect on Human Health and Remediation. *Egypt. J. Pet.*

2016, *25*, 107–123.

(29) US EPA. Method 550: Determination of Polycyclic Aromatic Hydrocarbons in Drinking Water By Liquid-Liquid Extraction and HPLC With Coupled Ultraviolet and Fluorescence Detection. **1990**, Method 550.

(30) US EPA. Method 610: Polynuclear Aromatic Hydrocarbons. **1997**, Method 610.

(31) Jones, C. L.; Bantz, K. C.; Haynes, C. L. Partition Layer-Modified Substrates for Reversible Surface-Enhanced Raman Scattering Detection of Polycyclic Aromatic Hydrocarbons. *Anal. Bioanal. Chem.* **2009**, *394*, 303–311.

(32) Cai, Y.; Yan, Z.; Yang, M.; Huang, X.; Min, W.; Wang, L.; Cai, Q. Polydopamine Decorated 3D Nickel Foam for Extraction of Sixteen Polycyclic Aromatic Hydrocarbons. *J. Chromatogr. A* **2016**, *1478*, 2–9.

(33) Colangeli, L.; Mennella, V.; Baratta, G. A.; Bussoletti, E.; Strazzulla, G. Raman and Infrared Spectra of Polycyclic Aromatic Hydrocarbon Molecules of Possible Astrophysical Interest. *Astrophys. J.* **1992**, *396*, 369–377.

(34) Sing, K. S. W. Reporting Physisorption Data for Gas/Solid Systems with Special Reference to the Determination of Surface Area and Porosity. *Pure Appl. Chem.* **1985**, *57*, 603–619.

(35) Lozhkomoev, A. S.; Glazkova, E. A.; Bakina, O. V; Lerner, M. I.; Gotman, I.; Gutmanas, E. Y.; Kazantsev, S. O.; Psakhie, S. G. Synthesis of Core–shell AlOOH Hollow Nanospheres by Reacting Al Nanoparticles with Water. *Nanotechnology* **2016**, *27*, 205603–205609.

(36) Zhang, L.; Lu, W.; Cui, R.; Shen, S. One-Pot Template-Free Synthesis of Mesoporous Boehmite Core-Shell and Hollow Spheres by a Simple Solvothermal Route. *Mater. Res. Bull.* **2010**, *45*, 429–436.

(37) Lerner, M. I.; Mikhaylov, G.; Tsukanov, A. A.; Lozhkomoev, A. S.; Gutmanas, E.; Gotman, I.; Bratovs, A.; Turk, V.; Turk, B.; Psakhye, S. G.; Vasiljeva, O. Crumpled Aluminum Hydroxide Nanostructures as a Microenvironment Dysregulation Agent for Cancer Treatment. *Nano Lett.* **2018**, *18*, 5401–5410.

(38) Férey, G.; Latroche, M.; Serre, C.; Millange, F.; Loiseau, T.; Percheron-Guegan, A. Hydrogen Adsorption in the Nanoporous Metal-Benzenedicarboxylate, MIL-53. *Chem. Commun.* **2003**, 2976–2977.

(39) Palik, E. D. *Handbook of Optical Constants of Solids*; Academic Press, 1985.

(40) Xiao, M.; Li, Y.; Allen, M. C.; Deheyn, D. D.; Yue, X.; Zhao, J.; Gianneschi, N. C.; Shawkey, M. D.; Dhinojwala, A. Bio-Inspired Structural Colors Produced *via* Self-Assembly of Synthetic Melanin Nanoparticles. *ACS Nano* **2015**, *9*, 5454–5460.

(41) Taflove, A.; Hagness, S. C. *Computational Electrodynamics: The Finite-Difference Time-Domain Method*, 3rd ed.; Artech House: Norwood, MA, 2005.